Role of p53 in the chronic pulmonary immune response to tangled or rod-like multi-walled carbon nanotubes

Katherine S. Duke, Elizabeth A. Thompson, Mark D. Ihrie, Alexia J. Taylor-Just, Elizabeth A. Ash, Kelly A. Shipkowski, Jonathan R. Hall, Debra A. Tokarz, Mark F. Cesta, Ann F. Hubbs, Dale W. Porter, Linda M. Sargent & James C. Bonner

View supplementary material

Published online: 14 Oct 2018.

Submit your article to this journal

Article views: 100

View Crossmark data

Taylor & Francis
Taylor & Francis Group

Check for updates

ARTICLE

Role of p53 in the chronic pulmonary immune response to tangled or rod-like multi-walled carbon nanotubes

Katherine S. Duke[a], Elizabeth A. Thompson[a], Mark D. Ihrie[a], Alexia J. Taylor-Just[a], Elizabeth A. Ash[b], Kelly A. Shipkowski[a], Jonathan R. Hall[a], Debra A. Tokarz[b], Mark F. Cesta[c], Ann F. Hubbs[d], Dale W. Porter[d], Linda M. Sargent[d] and James C. Bonner[a]

[a]Department of Biological Sciences, North Carolina State University, Raleigh, NC, USA; [b]College of Veterinary Medicine, North Carolina State University, Raleigh, NC, USA; [c]National Institute of Environmental Health Sciences, Research Triangle Park, NC, USA; [d]National Institute for Occupational Safety and Health, Morgantown, WV, USA

ABSTRACT

The fiber-like shape of multi-walled carbon nanotubes (MWCNTs) is reminiscent of asbestos, suggesting they pose similar health hazards when inhaled, including pulmonary fibrosis and mesothelioma. Mice deficient in the tumor suppressor p53 are susceptible to carcinogenesis. However, the chronic pathologic effect of MWCNTs delivered to the lungs of p53 heterozygous ($p53^{+/-}$) mice has not been investigated. We hypothesized that $p53^{+/-}$ mice would be susceptible to lung tumor development after exposure to either tangled (t-) or rod-like (r-) MWCNTs. Wild-type ($p53^{+/+}$) or $p53^{+/-}$ mice were exposed to MWCNTs (1 mg/kg) via oropharyngeal aspiration weekly over four consecutive weeks and evaluated for cellular and pathologic outcomes 11-months post-initial exposure. No lung or pleural tumors were observed in $p53^{+/+}$ or $p53^{+/-}$ mice exposed to either t- or rMWCNTs. In comparison to tMWCNTs, the rMWCNTs induced the formation of larger granulomas, a greater number of lymphoid aggregates and greater epithelial cell hyperplasia in terminal bronchioles in both $p53^{+/-}$ and $p53^{+/+}$ mice. A constitutively larger area of $CD45R^+/CD3^+$ lymphoid tissue was observed in $p53^{+/-}$ mice compared to $p53^{+/+}$ mice. Importantly, $p53^{+/-}$ mice had larger granulomas induced by rMWCNTs as compared to $p53^{+/+}$ mice. These findings indicate that a combination of p53 deficiency and physicochemical characteristics including nanotube geometry are factors in susceptibility to MWCNT-induced lymphoid infiltration and granuloma formation.

Introduction

The commercial use and incorporation of carbon nanotubes (CNTs) into consumer products has been on the rise because of their unique optical, electrical, and magnetic properties (Abdalla et al. 2015); however, little is known about the risks of possible exposure to these materials. Multi-walled carbon nanotubes (MWCNTs) possess some characteristics that are similar to asbestos, a known human carcinogen. For example, MWCNTs have a fiber-like shape and contain trace metal catalysts (e.g. Fe, Ni) from the manufacturing process (Donaldson et al. 2010; Poland et al. 2008). Physicochemical characteristics of MWCNTs, including their high aspect ratio, durability, biologic persistence, rigidity, and their ability to create chromosomal abnormalities are shared with asbestos and could influence their carcinogenic and fibrogenic potential (Duke and Bonner 2018; Siegrist et al. 2014; Nagai et al. 2011; Barrett et al. 1989; Hubbs et al. 2011).

There is concern that MWCNTs might behave like asbestos, which has been shown to cause pulmonary fibrosis and mesothelioma in humans and animal models. Like asbestos, MWCNTs delivered to the lungs of mice cause pulmonary fibrosis and lung cancer (Porter et al. 2010; Sargent et al. 2014). MWCNTs delivered to the lungs of mice by inhalation also cause interstitial, airway and sub-pleural fibrosis but not granulomas (Ryman-Rasmussen et al. 2009b), whereas oropharyngeal aspiration (OPA) causes both pulmonary fibrosis and granuloma formation (Muller et al. 2005; Dong et al. 2015; Duke et al. 2017). MWCNTs also reach the pleura of mice after inhalation or aspiration and

cause inflammatory lesions at the mesothelial lining and proliferation of mesothelial cells (Ryman-Rasmussen et al. 2009a; Xu et al. 2012; Mercer et al. 2013). Increased promotion of adenocarcinomas was reported in mice that were first exposed to the tumor initiator methylcholanthrene (MCA) followed by exposure to rod-like MWCNTs (Sargent et al. 2014). That study also showed serosal tumors morphologically consistent with sarcomatous mesotheliomas in five mice co-exposed to MCA and MWCNTs and in one mouse from the MCA control treatment group, but none resulting from MWCNT exposure alone.

There is some evidence to support the development of MWCNT-induced mesothelioma in rodent models. The administration of fibers by intraperitoneal (i.p.) injection in mice has been used as a surrogate to test mesothelioma development from the mesothelial cells on serosal surfaces. Administration of MWCNTs or asbestos to rodents by i.p. injection has also been shown to cause granuloma or mesothelioma on the lining of the abdominal cavity (Poland et al. 2008; Takagi et al. 2008). Mesothelioma formation has been shown 1 year post-i.p. injection of MWCNTs in tumor-susceptible heterozygous mice lacking one allele of the tumor suppressor p53 (p53$^{+/-}$); however, no comparison was done to wild-type p53 mice (p53$^{+/+}$) (Takagi et al. 2012). Mesothelioma has also been demonstrated in wild-type rats 1 and 2 years after MWCNT exposure by i.p. injection (Nagai et al. 2011; Rittinghausen et al. 2014). Furthermore, intrascrotal injection of MWCNTs has been shown to induce mesotheliomas in rats at time points shorter than 1 year following exposure (Sakamoto et al. 2009). There is little evidence for pleural mesothelioma in rodents by direct pulmonary exposure. Inhalation of rod-like MWCNTs in Fisher 344 (F344) rats induced lung cancer but not mesothelioma (Kasai et al. 2016), while intratracheal instillation of MWCNTs in F344 rats induced lung tumors and mesothelioma (Suzui et al. 2016). Inhaled MWCNTs reach the pleural space and are highly retained, thus having the potential to induce sustained pleural inflammation, mesothelial injury, and progressive subpleural fibrosis at this location (Ryman-Rasmussen et al. 2009a; Murphy et al. 2012; Xu et al. 2014b). However, the lack of evidence for mesothelioma in many mouse studies after MWCNT exposure may be due the

relative resistance of some mouse strains or due to different physicochemical features of MWCNT products. For example, one rod-like MWCNT product has been classified as having greater potential for carcinogenicity in humans compared to other MWCNTs International Agency for Research on Cancer (IARC) 2017].

Genetic alterations also play a part in the development of pulmonary diseases like lung cancer, mesothelioma, and fibrosis. The p53 tumor suppressor plays a key role in the regulation of the pulmonary carcinogenic and fibrotic processes by controlling cellular responses to stress including DNA repair, apoptosis, and cell cycle progression (Dai and Gu 2010). p53 plays a particularly important role in controlling cell proliferation (Agarwal et al. 1995). Mutation of either *p53* allele can lead to loss of both function and proliferation control, potentially resulting in fibrosis or cancer (Zilfou and Lowe 2009). Some disease states are associated with alteration of p53; for example, samples taken from patients with idiopathic pulmonary fibrosis (IPF) have high *p53* mutation incidences (Takahashi et al. 2002; Vancheri et al. 2010). Furthermore, the majority of IPF patients with overexpression of p53 have been found to have multiple point mutations in the *p53* gene (Hojo et al. 1998). Subchronic exposure (12 weeks) of transformed human lung epithelial cells to single walled CNTs *in vitro* resulted in neoplastic marker development and resistance to apoptosis via decreased p53 activation (Wang et al. 2011). Knock-down or knock-out of *p53* can increase tumor incidence and burden associated with decreased life span of the genetically modified mice (Wang et al. 2006, 2011; Xu et al. 2014a). p53 also plays a role in IL-17-induced tumor cell growth (Xu et al. 2014a). In addition, p53 acts cooperatively with NFκB to drive proinflammatory cytokine production (Lowe et al. 2014). Therefore, p53 is a crucial regulator of cellular homeostasis, and alterations of *p53* may result in the promotion of disease states in the lung.

To our knowledge, no studies have shown that direct pulmonary exposure of mice to MWCNTs, either by inhalation or OPA, results in mesothelioma in the absence of a tumor initiator. Additionally, despite the demonstrated role of p53 in pulmonary disease states, including carcinogenesis and fibrosis, the role of p53 in MWCNT-induced pulmonary

pathology has not been investigated. We hypothesized that p53-deficient mice would be susceptible to fibrosis or cancer following chronic exposure to MWCNTs. To evaluate the influence of physicochemical characteristics with emphasis on nanotube geometry, both tangled (t-) and rod-like (r-) MWCNTs were utilized for this study. Heterozygous p53-deficient (p53$^{+/-}$) mice were exposed to tMWCNTs or rMWCNTs via OPA and lung pathology was assessed 11 months post-initial exposure. While mesothelioma was not observed in p53$^{+/-}$ mice exposed to either tMWCNTs or rMWCNTs, we discovered that p53$^{+/-}$ mice were susceptible to MWCNT-induced granuloma formation and the formation of tertiary lymphoid tissue in lung tissue. Moreover, rMWNCTs caused significantly larger granulomas compared to tMWCNTs in wild-type (p53$^{+/+}$) mice and p53$^{+/-}$ mice.

Methods

Nanomaterial preparation

tMWCNTs were purchased from Helix Material Solutions Inc. (Richardson, TX) and were characterized previously (Ryman-Rasmussen et al. 2009a). rMWCNTs (XNRI MWCNT-7 05072001 K28) were manufactured by Mitsui & Co (Tokyo, Japan) and obtained from NIOSH. The MWCNTs used in this study have been previously characterized for residual trace metal content, diameter, length, surface area, zeta potential, and static bending ratio as an index of rigidity (Ryman-Rasmussen et al. 2009b; Porter et al. 2010; Mercer et al. 2011; Hilton et al. 2017; Duke et al. 2017). A summary of physicochemical characteristics of tMWCNT and rMWCNT is shown in Supplementary Table S1. MWCNTs were prepared in 0.1% Pluronic F-68 Solution (#P5556) from Sigma (St Louis, MO) and diluted with Dulbecco's phosphate-buffered saline (DPBS).

Animal care

Pathogen-free wild-type and p53$^{+/-}$ mice bred from a C57BL/6 background were purchased from the Jackson Laboratory (Bar Harbor, ME). Mice were housed in an IACUC-approved and AALAC-accredited animal facility. Animals were housed 1–5 per cage and fed LabDiet 5001 rodent diet and water *ad libitum*. All animal procedures were approved by the North Carolina State University IACUC.

Dosing of mice

Wild-type and p53$^{+/-}$ mice aged 8–12 weeks were dosed once a week for 4 weeks with 1 mg/kg tMWCNTs or rMWCNTs in 0.1% pluronic surfactant solution by OPA under isoflurane anesthesia. The cumulative dose of 4 mg/kg achieved by the four consecutive OPA doses of MWCNTs was chosen based on other previous studies (Porter et al. 2010; Sargent et al. 2014). Control mice received an equivalent dose volume of the vehicle, 0.1% pluronic surfactant solution. The control wild-type groups contained $N = 10$, the wild-type tMWCNT exposed group contained $N = 10$, the wild-type rMWCNT exposed group $N = 8$, the p53$^{+/-}$ control group $N = 14$, the p53$^{+/-}$ tMWCNT exposed group $N = 9$, and the p53$^{+/-}$ rMWCNT exposed group $N = 8$. The dosing strategy and animal numbers are summarized in Supplementary Figure S1.

Necropsy and collection of samples

Mice were euthanized utilizing pentobarbital i.p. injection 11 months post-initial exposure to tMWCNTs, rMWCNTs, or vehicle. Two 0.5 mL aliquots of DPBS were lavaged to collect bronchoalveolar lavage fluid (BALF) for cytokine and cellular content. The left lobe of the lung was inflated with approximately 500 μL neutral buffered formalin (Azer Scientific, Morgantown, PA) and fixed overnight, dehydrated in 70% ethanol overnight, then embedded in paraffin for histology and the right lobes were divided equally into RNAlater (Fisher Scientific, Waltham, MA) or snap frozen in a cryotube for mRNA and protein analysis, respectively.

Bromodeoxyuridine (BrdU) immunohistochemical staining (IHC)

To label cells actively synthesizing DNA, intraperitoneal injections of 100 mg/kg BrdU (Sigma) in DPBS were administered to mice 1-h prior to euthanasia. Lungs and small intestine (positive control) were sectioned at 5 μm using a microtome, mounted on a negatively charged slide and stained using a protocol described previously (Duke et al. 2017).

Pleural lesion analysis

Three lung sections from each mouse were cut and stained with H&E. The visceral pleura was carefully evaluated for inflammatory, fibrotic or carcinogenic lesions in all sections consistent with our previous analysis of pleural lesions after MWCNT inhalation in C57BL/6 mice (Ryman-Rasmussen et al. 2009a).

Granuloma analysis

Trichrome-stained lung sections containing granulomas were imaged with a respective scale bar. Each granuloma was characterized by both the presence of MWCNTs in the tissue and an associated inflammatory reaction to them consisting of epithelioid macrophages and/or fibrosis. The presence of MWCNTs within alveolar macrophages with no associated fibrosis or epithelioid macrophages was not considered a granuloma. Adobe Systems Incorporated, San Jose, CA was utilized to measure granuloma area by using the ruler tool to measure and set a custom measurement scale by converting pixels to micrometers (μm). The lasso tool was used to encompass the granuloma. A granuloma was defined as a mass of cells (mainly epithelioid macrophages) surrounding a foreign body. Each granuloma area was measured using Photoshop software and tracing around the easily defined border excluding surrounding epithelial cells (Schneider et al. 2012). Total lung section area was measured by first combining lung images using the image stitching plugin available through the Fiji image processing package distributed by ImageJ https://imagej.net/ImageJ) following a previously described method (Preibisch et al. 2009). The area of the lung was then measured using the lasso tool after being set to the dimensions of the image.

Lymphoid tissue quantification analysis

Three lung sections from each mouse were cut, stained with bromodeoxyuridine (BrdU) and analyzed for inducible bronchus-associated lymphoid tissue (iBALT) or ectopic lymphoid tissue (ELT) formations by scanning these sections for lymphoid structures. Each iBALT or ELT identified was imaged and the area was measured using the lasso tool in Photoshop from BrdU IHC-stained slides. Total lung section area was measured from BrdU IHC-stained mouse lungs that were imaged at 40× and stitched together using the ImageJ stitching plugin in Fiji (Preibisch et al. 2009). The total lung section area was quantitatively measured in ImageJ as were all lymphoid aggregates of more than 10 mononuclear cells. These were put into categories of iBALT or ELT for further analysis. The total number of iBALT or ELT formations and the number containing BrdU-positive cells were counted. The number of granulomas adjacent to lymphoid tissue were also counted using the H&E-stained sections.

Lymphoid tissue characterization

Three lung tissue blocks from each genotype and treatment group were selected for IHC staining of a T-cell marker, CD3, and a pan B-cell marker, CD45R/B220, to assess lymphoid tissue structure. The anti-CD3 antibody (Cat# A0452) was purchased from Dako (Carpinteria, CA) and the anti-CD45R antibody (Cat# 550286) was purchased from BD Biosciences (San Jose, CA).

Hyperplasia analysis at first terminal bronchial duct bifurcation

Images were taken at 100× of the first bronchial duct bifurcation from BrdU immunohistochemically stained lung sections. These images were centered to keep imaging consistent; some mouse lungs did not have these structures in the sections, thus not every animal is represented. The nuclei of cuboidal epithelial cells lining the airway and at the bifurcation were counted. Brown nuclei positive for BrdU incorporation were then also counted and are reported as the percent BrdU-positive epithelial cells at the terminal bronchial duct bifurcation.

Collagen Analysis

Snap frozen right lung lobes were weighed out to 10 mg, homogenized and assayed for protein and soluble collagen. The Sircol-soluble collagen kit (Biocolor, Carrickfergus, UK) was used to assay collagen content and the Pierce BCA protein assay (Thermo Scientific, Waltham, MA) was used to determine protein concentrations from each mouse lung. Area-to-perimeter ratio analysis was also conducted utilizing Masson's Trichrome-stained mouse

lungs by quantitatively measuring collagen surrounding the airways as described previously (Duke et al. 2017).

Inflammatory quantification

BALF was collected and 100 μL was cytospun onto slides. Cells were stained with the DiffQuik® stain set (Dade Behring Inc, Newark, DE). A differential cell count was performed on the BALF to determine the percentage of macrophages, eosinophils, neutrophils, and lymphocytes. A total of 500 cells were counted per slide.

Cytokine quantification

Cytokines (total TGF-β1, osteopontin, and PDGF-BB) from BALF were measured by commercially available DuoSet enzyme-linked immunosorbent assay (ELISA) kits (R&D Systems, Inc., Minneapolis, MN).

Transmission electron microscope (TEM)

As purchased, tMWCNTs and rMWCNTs were imaged using a JEOL 2000FX scanning TEM and samples were prepared as described previously (Dandley et al. 2015). Lung tissue from mice exposed to either tMWCNTs or rMWCNTs was first fixed with formalin and embedded in paraffin then submitted to core TEM facilities for de-paraffinization and resin embedding. TEM of MWCNTs in lung tissue was performed as described previously (Ryman-Rasmussen et al. 2009a).

Statistical analysis

Statistical analysis was done using GraphPad Prism software version 5.0 (GraphPad Software, Inc., San Diego, CA). A one-way ANOVA with a Tukey *post hoc* test was performed to determine statistical differences between treatments and genotypes.

Results

Survival

All mice survived to the end of the study with the exception of three (Supplementary Figure S1). Two male mice in the p53$^{+/-}$ group treated with rMWCNT died early from unknown causes and
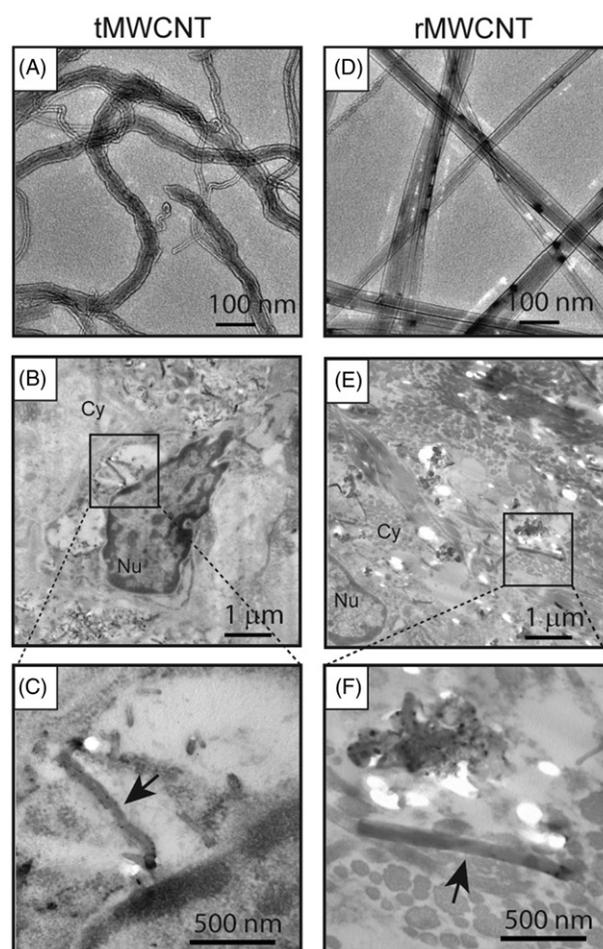

Figure 1. TEM images of nanomaterials used in the study. (A) tMWCNTs and (D) rMWCNTs. (B) TEM image of tMWCNTs in lung granuloma from a p53$^{+/-}$ mouse at 11 months post-exposure. Cy indicates cytoplasm, and Nu indicates the nucleus. (C) Inset showing a representative tMWCNT (arrow) near the nuclear membrane of a phagocytic cell. (E) TEM image of rMWCNTs in granulomatous connective tissue from a p53$^{+/-}$ mouse at the end of the 11-month study period. (F) Inset showing a representative rMWCNT (arrow).

one female mouse in the p53$^{+/-}$ group treated with tMWCNT was euthanized due to lymphoma formation.

MWCNTs in the lung tissue of mice 11 months post-initial exposure

Transmission electron microscopy (TEM) of the bulk nanomaterials used in this study showed the contrasting geometric shapes between 'tangled' tMWCNTs and 'rod-like' rMWCNTs (Figure 1(A,D). Singlet and agglomerated nanotube structures were present within pulmonary alveolar macrophages 11 months post-initial exposure to either t- or r-MWCNTs (Figure 1(B,C,E,F)). tMWCNTs were present intracellularly and within close proximity to the
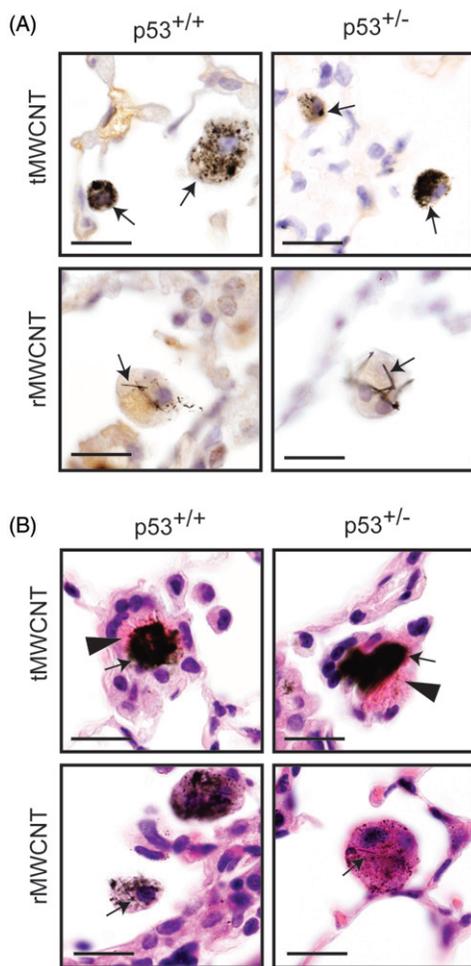
tMWCNT panels). No crystalline bodies were observed in mouse lungs exposed to rMWCNTs.

Inflammatory cells and cytokines in BALF

Macrophages dominated the immune cells in the BALF from mouse lungs from both genotypes and treatment groups. Though there was a slight increase in neutrophil cell counts from the lungs of $p53^{+/+}$ mice with rMWCNT exposure, this increase was not significant (data not shown). Analysis of the cellular makeup of the BALF revealed that control, tMWCNT- or rMWCNT-exposed mice contained similar total cell counts (data not shown). Differential cell counts conducted on the cytospins of the BALF revealed predominantly macrophage-populated lungs with a slight, but not significant, increase in lymphocytes and neutrophils in lungs treated with rMWCNTs (data not shown). Cytokine levels of osteopontin (OPN), TGF-β1, and PDGF-BB in the BALF were not significantly increased by either MWCNT type or different between $p53^{+/+}$ and $p53^{+/-}$ mice at the chronic endpoint evaluated in this study (data not shown).

Granuloma formation in the lungs of $p53^{+/+}$ and $p53^{+/-}$ mice chronically exposed to tMWCNTs or rMWCNTs

Mice exposed to tMWCNTs had multiple small granulomas mostly confined to the distal terminal bronchioles and alveolar ducts in the centriacinar region near the alveolar-bronchiolar junctions (Figure 3(A)). There was a trend towards larger granuloma number and total granuloma area in t- or rMWCNT-exposed $p53^{+/-}$ mice compared to $p53^{+/+}$ mice, although this difference was not statistically significant (Figure 3(B,C)). The macrophages containing t- or r- MWCNTs were enlarged with vacuolated cytoplasm, though the compacted agglomerates of tMWCNTs frequently obscured the macrophages. There were occasional multinucleated giant macrophages in the lungs of both $p53^{+/+}$ and $p53^{+/-}$ mice treated with either tMWCNTs or rMWCNTs. The locations of the granulomas associated with rMWCNTs were similar to the location of the granulomas seen with tMWCNT-exposed animals. The granulomas associated with rMWCNTs were qualitatively larger with greater cellularity compared to

Figure 2. Pulmonary alveolar macrophages containing tMWCNTs or rMWCNTs in the lungs of mice at the end of the 11-month study period. (A) Hematoxylin-stained mouse lung tissue from both wild-type and $p53^{+/-}$ with arrows indicating the enclosed foreign material within the alveolar macrophages in the lungs (scale bars = 20 μm). (B) Hematoxylin & Eosin-stained (H&E) lung tissue from wild-type and $p53^{+/-}$ mice with arrows indicating macrophages containing tMWCNTs or rMWCNTs. Arrowheads indicate crystalline bodies within the cytosol of alveolar macrophages (scale bars = 20 μm).

Golgi apparatus and the nuclear membrane, but not within the nucleus. rMWCNTs were also present intracellularly 11 months post-initial exposure and were found in singlet and in condensed aggregates. Light microscopy of lung sections from mice showed aggregates and singlets of tMWCNTs or rMWCNTs within alveolar macrophages (Figure 2(A)). Of note, the rMWCNTs, but not the tMWCNTs, protruded from macrophages indicating frustrated phagocytosis (Figure 2(A)). In addition, crystalline bodies in the cytosol of alveolar macrophages were observed in the lungs of either $p53^{+/+}$ or $p53^{+/-}$ mice exposed to tMWCNTs (Figure 2(B), arrows in
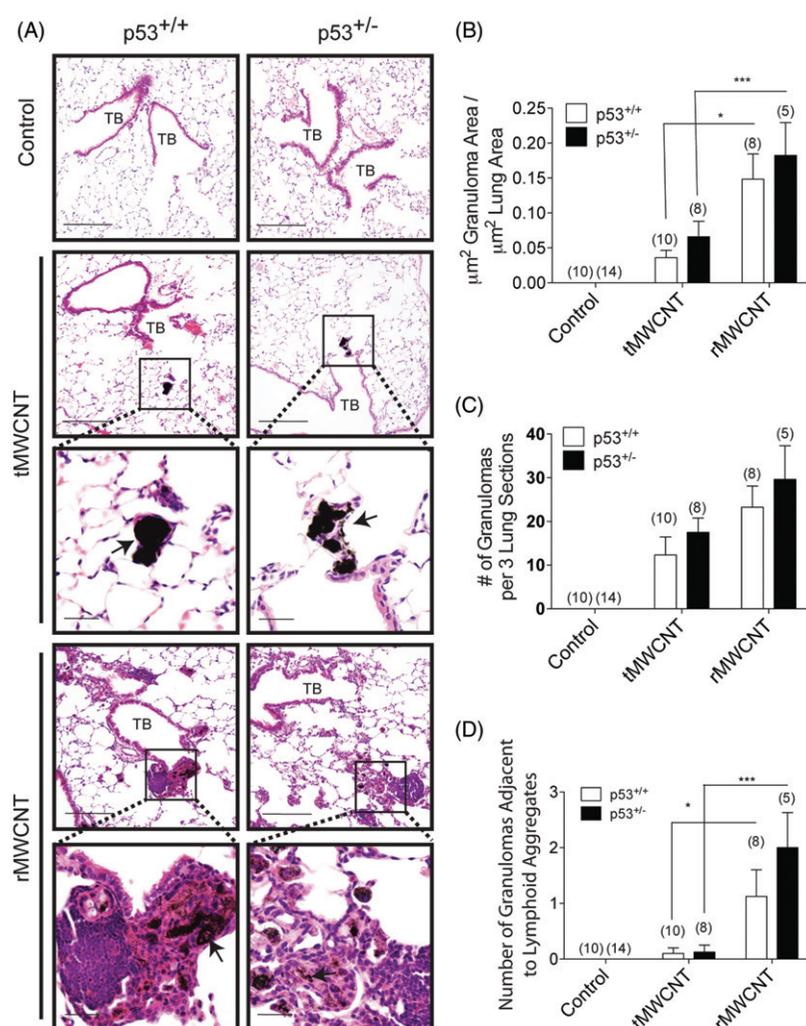
Figure 3. rMWCNT exposure results in significantly larger lung granuloma area and a higher association with lymphoid tissue compared to tMWCNT, with a trend of larger formations in the lungs of p53$^{+/-}$ mice. (A) H&E-stained lung sections from wild-type and p53$^{+/-}$ mouse lungs exposed to t- or r- MWCNTs near the terminal bronchioles (TB) of the lungs. Insets depict matured granuloma formations as indicated by arrows (scale bars = 200 μm, inset scale bars = 50 μm). (B) Average area of lung occupied by granuloma measured by quantitative morphometry (***$p < 0.001$, *$p < 0.05$ between tMWCNTs and rMWCNTs). (C) Average number of granulomas per three lung sections per mouse. (D) Average number of granulomas directly adjacent to lymphoid tissue per three lung sections per mouse. Number in parentheses above graph bar indicates number of animals per group. (***$p < 0.001$, *$p < 0.05$ between tMWCNTs and rMWCNTs).

tMWCNTs, these granulomas contained numerous macrophages and often surrounded by lymphocytes (Figure 3(A)). Rarely, there were rMWCNT-laden macrophages within the airway wall surrounded by increased numbers of fibroblasts. Foci of iBALT were observed near bronchioles with adjacent granulomas in the lungs of both p53$^{+/+}$ and p53$^{+/-}$ mice exposed to rMWCNTs but not tMWCNTs (Figure 3(D)). Of note, there were significantly more granulomas adjacent to lymphoid tissue in the rMWCNT-exposed mouse lungs compared to the tMWCNT-exposed mouse lungs, and there was no notable difference between genotypes (Figure 3(D)).

Effect of p53 deficiency and MWCNT treatment on lymphoid tissue formation

Bronchus-associated lymphoid tissue (BALT) is a tertiary lymphoid structure composed of lymphocytes (i.e. T and B cells) mainly along bifurcations of the upper airways and rarely forms in healthy human or mouse lungs. Inducible BALT (iBALT) can be induced during chronic inflammation, infection or other disease states (Sminia et al. 1989; Foo and Phipps 2010). Both iBALT and non-bronchus-associated ELT structures were observed in mice from this study (Figure 4(C,D)). The total number of lymphoid aggregates (iBALT and ELT) in tMWCNT-exposed mice was
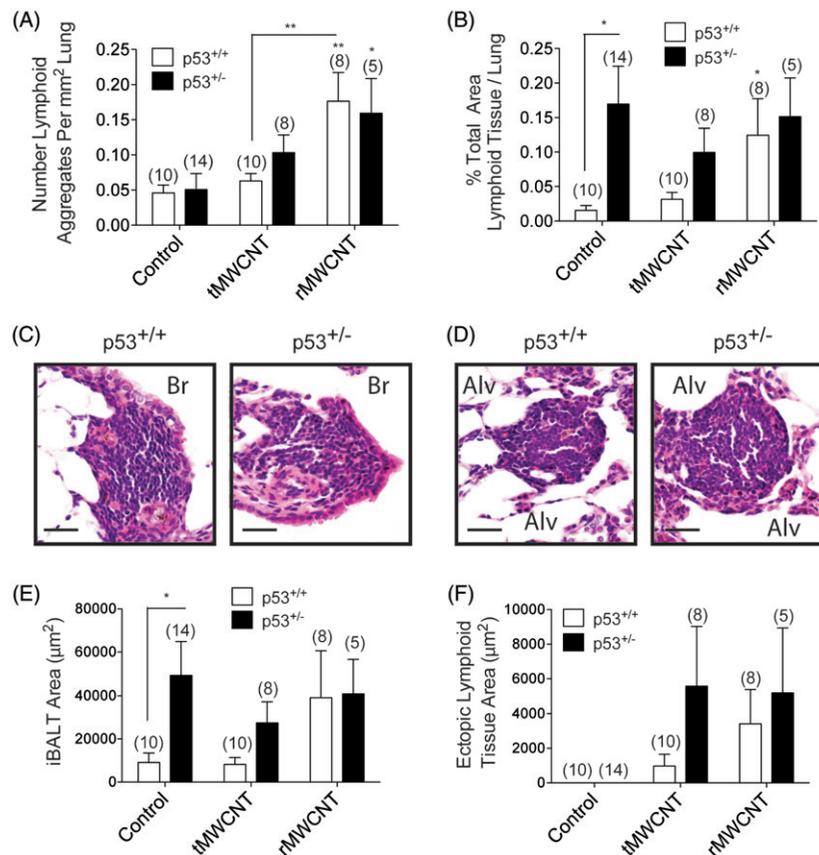
Figure 4. Formation of inducible lymphoid tissue in response to tMWCNT or rMWCNT exposure. (A) Average number of lymphoid aggregates as a function of square mm lung area (**$p < 0.01$ between tMWCNT and rMWCNT, **$p < 0.01$, *$p < 0.05$ compared to control). (B) Average percent of lung area occupied by lymphoid tissue measured by quantitative morphometry (*$p < 0.05$ between genotypes, *$p < 0.05$ compared to control). (C) Inducible bronchus associated lymphoid tissue (iBALT) along the bronchial (Br) airway and (D) ectopic lymphoid tissue (ELT) and surrounding alveolar (Alv) space of the lung of a wild-type and p53$^{+/-}$ mouse lung exposed to rMWCNTs (scale bars = 50 μm). Lymphoid tissue area broken up into average area of (E) iBALT and (F) ELT (*$p < 0.05$ between genotypes). Number in parentheses above graph bar indicates number of animals per group.

similar to that seen in the control animals, although there was a trend for increased numbers of lymphoid aggregates in p53$^{+/-}$ mice compared to p53$^{+/+}$ (Figure 4(A)). The number of lymphoid aggregates significantly increased following rMWCNT, but induction of lymphoid aggregates by rMWCNTs was not different between p53$^{+/+}$ and p53$^{+/-}$ genotypes (Figure 4(A)). The percent of the lung occupied by lymphoid tissue, as measured by semi-quantitative morphometry, was significantly greater in control p53$^{+/-}$ mice compared to control p53$^{+/+}$ mice, but was not further increased by tMWCNT or rMWCNT treatment (Figure 4(B)). Taken together, these data suggest that while rMWCNTs increased the number of lymphoid aggregates, the area of lung occupied by these lymphoid structures was greater in p53$^{+/-}$ mouse lungs primarily due to constitutive iBALT in the absence of MWCNT exposure (Figure 4(E,F)). iBALT lesions contained proliferating cells as observed

with BrdU IHC staining, yet proliferation was similar in p53$^{+/+}$ and p53$^{+/-}$ mouse lungs regardless of MWCNT treatment (data not shown). Overexpression of cytokines like IL-6 are associated with inducing iBALT Goya et al. 2003, yet we did not observe increased levels of IL-6 mRNA from treated mouse lung samples, nor did we detect increased transcription of chemokines: CCL2 (C–C motic ligand 2), CXCL10 (C–X–C motif chemokine 10) and CXCL9 (C–X–C motif chemokine 9) at this time point (data not shown).

Structural organization of inducible tertiary lymphoid tissue

To further characterize the lymphoid aggregates and granulomas, IHC stains for T cells (CD3^{+}) and B cells (CD45R^{+}/B220) were applied to serial lung sections. The cellular make-up of the inducible
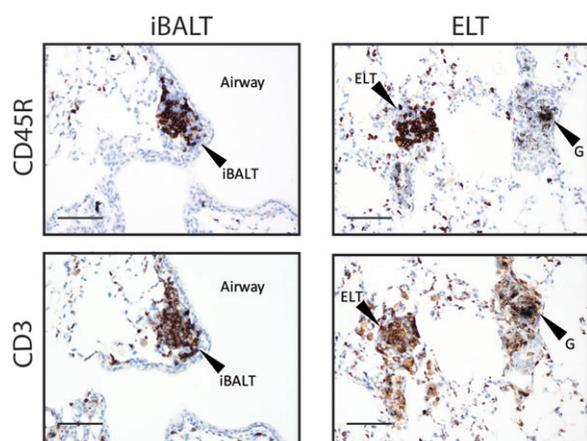
Figure 5. Structure of pulmonary inducible lymphoid tissue. Lung tissue from p53$^{+/−}$ mice exposed to rMWCNTs for 11 months was immunohistochemically stained for the T-cell marker CD3 and the B cell marker CD45R (B220) depicting a B cell germinal center with peripheral T cells in both the iBALT and ELT formations. For reference a granuloma (G) is indicated to show negative staining of cellular aggregates (scale bars = 100 μm).

lymphoid tissues (iBALT and ELT) was classically ordered with a centrally aggregated CD45R$^+$ B cell population surrounded by more loosely distributed CD3$^+$ T cells (Figure 5). Despite nonspecific staining of macrophage cytoplasm for CD3, close examination of the cellular morphology revealed that T and B cells were common in the periphery of both the r- and tMWCNT-induced granulomas (data not shown). Prior studies of MWCNT exposure have shown increased T cell and macrophage staining around granulomas as well (Huizar et al. 2011, 2013).

rMWCNT exposure resulted in increased DNA synthesis in cells within granulomas

Lung tissue stained with BrdU was analyzed for brown-staining nuclei within granulomas that indicated proliferation (Figure 6(A)). Each granuloma counted was validated by the presence of MWCNTs as described in the methods section. About 25% of the p53$^{+/+}$ and 15% of the p53$^{+/−}$ granulomas resulting from rMWCNT-exposure included BrdU-positive cells compared to only 5% of either p53$^{+/+}$ or p53$^{+/−}$ tMWCNT-resulting lung granulomas (Figure 6(B)).

Bronchiolar epithelial hyperplasia induced by MWCNT exposure

Bronchiolar epithelial hyperplastic lesions were observed in the lungs of both p53$^{+/+}$ and p53$^{+/−}$
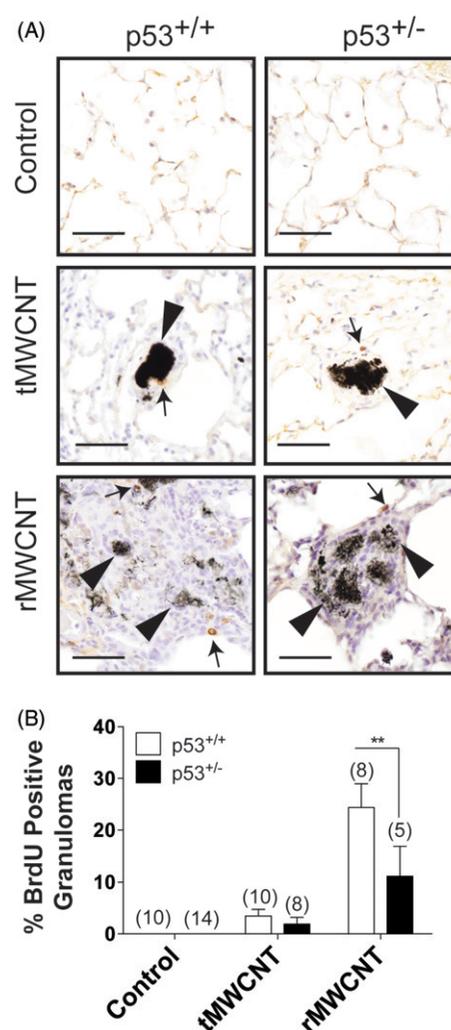

Figure 6. BrdU IHC staining of mouse lungs from control and MWCNT-resultant granulomas show increased proliferation with rMWCNT exposure. (A) Tissue from wild-type and p53$^{+/−}$ mouse lungs exposed to t- or rMWCNTs for 11 months was stained with BrdU where a dark brown stain indicates DNA synthesis and is also indicated by arrows. Arrowheads indicate the nanomaterial within the granuloma (scale bars = 50 μm). (B) Average number of granulomas with BrdU positively stained nuclei ($^{**}p < 0.01$ between genotypes). Number in parentheses above graph bar indicates number of animals per group.

mice exposed to rMWCNTs, but were rarely observed in tMWCNT-exposed mouse lungs (Figure 7(A)). Hyperplasia was measured by quantifying BrdU-positive bronchiolar epithelial cells. Quantification of BrdU-positive epithelial cells along the first bronchoalveolar duct bifurcation revealed increased proliferation in rMWCNT-exposed p53$^{+/+}$ and p53$^{+/−}$ mouse airway epithelial cells compared to control or tMWCNT treatment groups (Figure 7(B)). There were also occasional aggregates of plasma cells near airways of rMWCNT-exposed mice, which
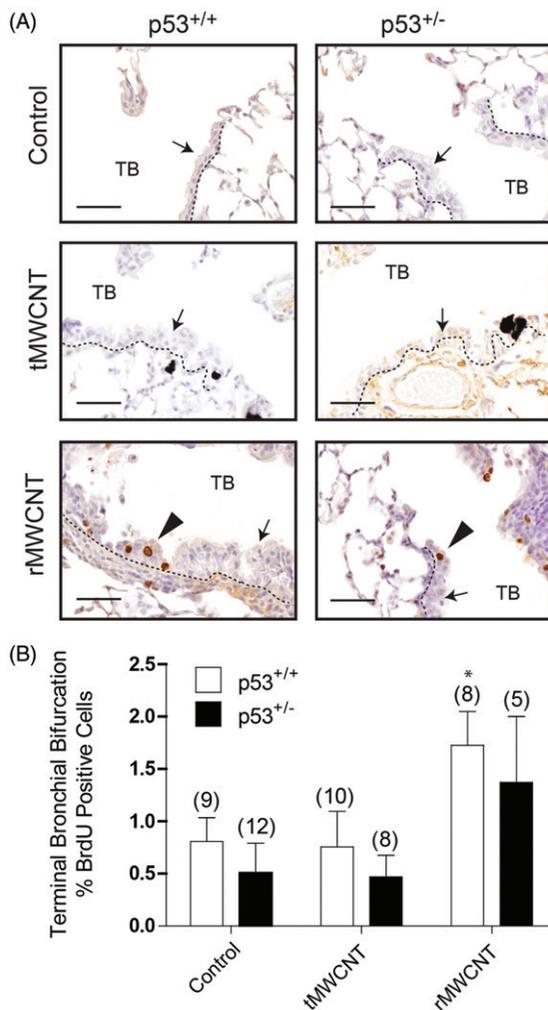
(A)

(B)

Figure 7. Bronchiolar hyperplasia. (A) BrdU stained lung sections from control, tMWCNT and rMWCNT wild-type and p53$^{+/-}$ mice were imaged to show the bronchial epithelium near a terminal bronchiole (TB) as indicated by arrows. Arrowheads indicate BrdU-positive epithelial cells in the hyperplastic epithelium (scale bars = 50 μm). (B) Quantitation of BrdU-positive epithelial cells at the terminal bronchial bifurcation reported as %BrdU-positive cells with standard error. Numbers in parenthesis indicate the number of animals analyzed per group ($^*p < 0.05$ compared to control).

were not seen in the control or tMWCNT-exposed mouse lungs. In the animals exposed to rMWCNTs, there was a markedly increased incidence of bronchiolar epithelial hyperplasia at terminal bronchioles and a few instances of alveolar hyperplasia. Airway epithelial hyperplasia coupled with papillary hyperplasia (projection of epithelial cells into the lumen of the airway with simple connective tissue core present), could mark the transition towards neoplasia (Renne et al. 2009). A papillary hyperplastic lesion in a small airway was observed in CD45R- and CD3-stained serial sections from a p53$^{+/-}$ mouse exposed
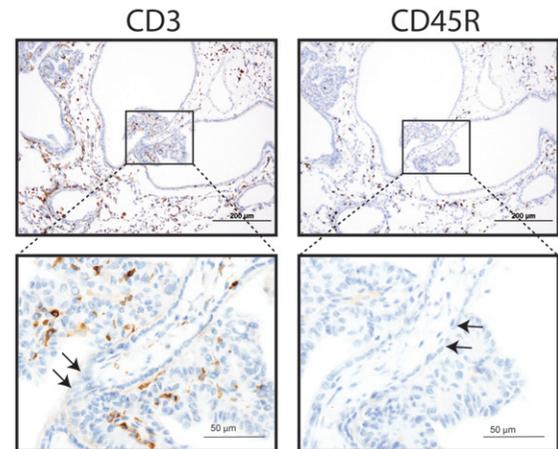

Figure 8. Papillary hyperplasia of the bronchiolar epithelium at alveolar duct bifurcation. Serial sections of papillary hyperplasia at the terminal bronchus in a p53$^{+/-}$ mouse 11 months post-initial exposure to rMWCNTs. This rare pathology was captured in the IHC T-cell marker CD3 and B cell marker CD45R sections. Arrows indicate location of papillary attachment to the bronchiole wall (scale bars = 200 μm, inset scale bars = 50 μm).

to rMWCNTs (Figure 8). Epithelial hyperplasia was a feature of rMWCNT-exposed mouse lungs, although differences between genotypes were not identified. However, the only evidence of papillary hyperplasia was found in one p53$^{+/-}$ mouse exposed to rMWCNTs.

Pulmonary fibrosis after chronic exposure to tMWCNTs or rMWCNTs

Regional fibrosis was evident in Trichrome-stained lung sections from mice exposed to MWCNTs, primarily located within granulomas (Figure 9(A)). rMWCNTs induced larger collagen-laden granulomas compared to tMWCNTs in both p53$^{+/+}$ and p53$^{+/-}$ mice. To determine if significant collagen deposition occurred after exposure to tMWCNTs or rMWCNTs, a quantitative Sircol assay was used to measure total lung collagen. Also, a semi-quantitative morphometric (area to perimeter ratio) analysis was performed to measure airway fibrosis. There was no significant difference in airway fibrosis (area to perimeter ratio) based on quantitative morphometry performed using the airway to perimeter ratio method (data not shown). The Sircol assay showed no difference in total collagen content from the lungs of p53$^{+/+}$ versus p53$^{+/-}$ mice (Figure 9(B)). Moreover, there was no difference between genotypes in the tMWCNT exposure group. While p53$^{+/-}$ mice had significantly

Discussion

The aim of this study was to examine the inflammatory, fibrogenic, and carcinogenic potential of two types of MWCNTs with differing geometry (tangled versus rod-like) in the lungs of transgenic mice deficient in one allele of tumor suppressor p53. Because rMWCNTs have been classified as a Group 2B possible human carcinogen (IARC 2017), we postulated that chronic exposure to these rod-like nanotubes would cause lung cancer or mesothelioma in p53$^{+/-}$ but not wild-type p53$^{+/+}$ mice. No MWCNT-related lung tumors or mesothelioma were observed in p53$^{+/-}$ mice, although rMWCNTs caused focal bronchiolar epithelial hyperplasia in p53$^{+/-}$ mouse lungs. Moreover, rMWCNTs caused more robust granuloma formation compared to tMWCNTs and there was a trend towards larger granulomas in p53$^{+/-}$ mice. Interestingly, we observed that rMWCNTs, but not tMWCNTs, stimulated iBALT formation in p53$^{+/+}$ mice and iBALT was spontaneously generated in the lungs of p53$^{+/-}$ mice. Also, p53$^{+/-}$ mice exhibited significantly larger lung area obscured by lymphoid aggregates compared to p53$^{+/+}$ mice. Overall, our findings indicate that p53 plays a role in constitutive iBALT formation in the lungs of mice and regulates rMWCNT-induced granuloma size.

Our study revealed a role for p53 in regulating granuloma formation after exposure to MWCNTs. The observation of increased BrdU-positive cells in granulomas from p53$^{+/+}$ or p53$^{+/-}$ mice after chronic exposure to rMWCNT is indicative of continual injury and/or immune stimulation. We observed that T cells were integrated into the granulomas induced by rMWCNTs (Figure 5) and this is indicative of previously described immune granulomas that are positive for CD205, a marker of antigen-presenting cells (Ohtani 2013). Our observation of T-cell infiltration within foreign body granulomas containing MWCNTs and the proximity of iBALT or ELT to many of these granulomas, especially in p53$^{+/-}$ mice, suggest ongoing immune responses in the lung tissue of rMWCNT-exposed mice.

The development of tertiary lymphoid tissues (iBALT and ELT) appears to be due to a combination of p53 deficiency and rMWCNT exposure in the lung. These foci form in response to chronic inflammation, infection, or other disease states (Foo
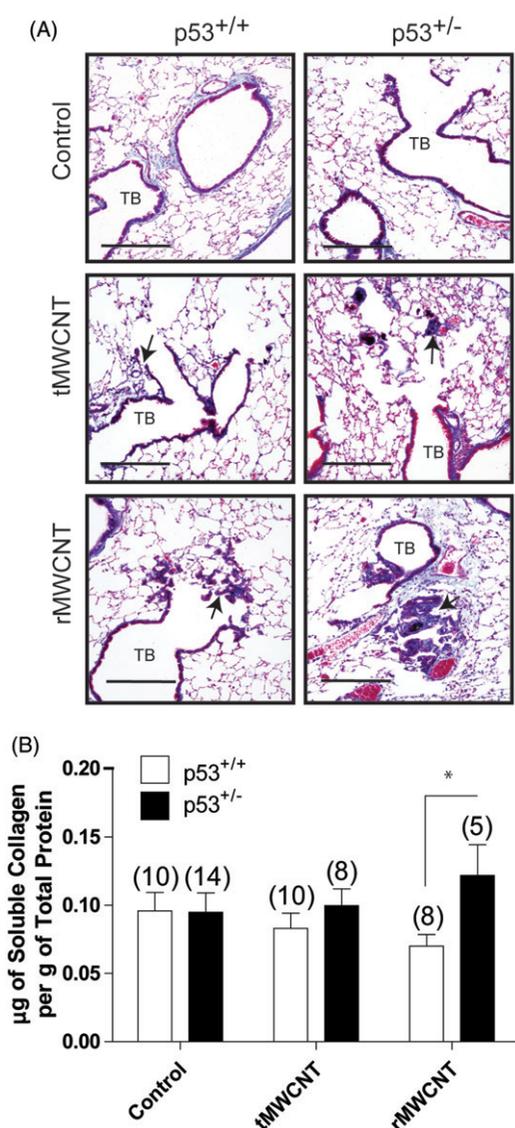

Figure 9. Collagen deposition 11 months following initial tMWCNT or rMWCNT pulmonary exposure. (A) Trichrome-stained lung sections are imaged here depicting terminal bronchioles (TB). Arrows indicate fibrotic foci (scale bars = 200 μm). (B) Relative average μg of soluble collagen per mouse lung as determined using the Sircol assay (*$p < 0.05$ between genotypes). Number in parentheses above graph bar indicates number of animals per group.

greater lung collagen content compared to p53$^{+/+}$ mice in the rMWCNT treatment group, this was due to a reduction in total lung collagen content in p53$^{+/+}$ mice exposed to rMWCNT.

Pleural lesions

No evidence of pleural inflammation or mesothelioma was found in either p53$^{+/+}$ or p53$^{+/-}$ mice after careful examination of three H&E-stained sections per lung (data not shown).

and Phipps 2010; Aloisi and Pujol-Borrell 2006). The early development of this tissue is driven by IL-1α, and IL-1-receptor deficient mice fail to develop iBALT following exposure to either aluminum salts, silica, or viruses (Kuroda et al. 2016; Neyt et al. 2016). IL-6 also appears to play a role in the development of lymphoid-like structures in the lung (Goya et al. 2003). Interestingly, silica-induced lymphoid neogenesis can result in the development of an induced autoimmune phenotype (Bates et al. 2015). The lymphoid neogenesis exhibited in our study contained cellular elements organized into *de novo* formations of a B cell follicle surrounded by T cells (Aloisi and Pujol-Borrell 2006). Additionally, increased iBALT in the lung is observed in mice as they age, and is further exacerbated by particulates found in cigarette smoke (John-Schuster et al. 2015). Previous examination of pulmonary exposure to rMWCNTs found that exposure resulted in the dilation of pulmonary lymphatics after 56 days as measured by indirect immunofluorescence of podoplanin, a lymphatic endothelial marker (Porter et al. 2010). Prior studies have observed MWCNTs deposited into BALT and have shown that these lymphoid tissues are a slower clearance method compared the mucociliary escalator in a rat model (Aiso et al. 2010). To date, there is no current literature available on p53 regulation or involvement of inducible lymphoid tissue development; however, p53 has been implicated in the immune response during development. For example, the co-regulatory function of NFκB and p53 increases IL-6 in primary human monocytes and macrophages and induces neutrophil chemokines (Lowe et al. 2014). In addition, following pulmonary infection with gram-negative bacteria, p53 null or inhibited mice were able to clear the infection more quickly compared to wild-type mice (Madenspacher et al. 2013). This clearance was due to increased phagocytosis, degranulation and NOX-dependent oxidant generation by neutrophils, yet these mice also exhibited high mortality following infection and clearance due to aggravated lung injury. It is possible that the increased iBALT formations observed in p53$^{+/-}$ mice in the present study could result in an altered immune microenvironment that could favor tumor development.

We observed that alveolar macrophages contained tMWCNTs or rMWCNTs at the end of our chronic study. Murine alveolar macrophages are a very long-lived cell, with a life-span that may potentially be as long as the animal itself (Murphy et al. 2008). Therefore, it was not surprising to observe MWCNTs in macrophages at nearly a year after exposure; i.e. approximately half the life span of the animal. In our study, the observation of BrdU-positive macrophages in granulomatous formations resulting from rMWCNT- and not from tMWCNT-exposure lends itself to suggest that chronic injury by rMWCNTs could signal macrophage replenishment. Alveolar macrophages generally have a low proliferative index under normal homeostatic conditions, although they can self-replenish their population when the need arises during or following injury (Hashimoto et al. 2013). Infiltrating monocytes are also a source of macrophage replenishment in the lung as these cells differentiate into mature alveolar macrophages. Interestingly, alveolar macrophages from the lungs of p53$^{+/+}$ or p53$^{+/-}$ mice exposed to tMWCNTs-contained crystalline bodies, but these bodies were not observed in macrophages from mice exposed to rMWCNTs. A study by K⊘bler et al. (2015) evaluated the pulmonary toxicity of a short, tangled MWCNT and two longer, thicker MWCNTs (one of which was Mitsui-7) at 1, 3 and 28 days and found crystalline bodies, described as eosinophilic crystalline pneumonia, within the cytosol of alveolar macrophages from mice exposed to all types of MWCNTs studied, but primarily in mice exposed to longer thicker MWCNTs. They also reported that carbon black nanoparticle exposure did not increase crystal incidence above that seen in control animals and suggested that increased development of crystals might be related to shape and dimensions of carbon-based particles. In the present study, we observed crystalline bodies in macrophages from mice exposed to tMWCNT but not rMWCNTs. However, we assessed only a single chronic time point, so it is possible that crystalline bodies, if similar to the crystal structures described by K⊘bler et al. (2015), could have been formed in lungs of rMWCNT-exposed mice early on, but resolved by the 11-month time point.

A major issue that we sought to address in this study was to determine if p53$^{+/-}$ mice, a mouse model that is susceptible to tumor development, would develop mesothelioma after pulmonary exposure to MWCNTs. Previous studies of p53$^{+/-}$

mice injected intraperitoneally with asbestos or rMWCNTs demonstrated more rapid development of mesotheliomas resulting from MWCNT compared to asbestos (Takagi et al. 2008, 2012). We did not observe mesothelioma or other exposure-related neoplasms 11 months following the initial dose delivered by OPA in either wild-type or p53$^{+/-}$ mice. Mesothelioma has been observed in mice following direct pulmonary exposure to asbestos. For example, Bozelka et al. (1983) used Balb/C mice and long-term inhalation exposure to chrysotile asbestos (2 h/day for 75 days) and demonstrated >90% of the animals developed tumors at the visceral pleura after 12–18 months (Bozelka et al. 1983). However, 10% of control (air exposed) Balb/C mice in that study developed tumors, suggesting that Balb/C mice are susceptible to tumor formation compared to the C57BL/6 strain used in our study. In addition, DBA/2J mice are more susceptible than C57BL/6 mice to aflatoxin-induced carcinogenesis (Hunter 2012). Therefore, it is not surprising that mesothelioma was not observed in p53$^{+/-}$ mice on a C57BL/6 background after MWCNT exposure in the present study. Overall this may indicate that mice, even transgenic strains that are susceptible to tumor promotion, are poor models for assessing the carcinogenic potential of MWCNTs. A study by Chernova et al. (2017) elegantly demonstrated mesothelioma on the chest wall (parietal pleura) of C57BL/6 mice after direct intrapleural injection of long MWCNTs or long asbestos fibers. However, intrapleural injection by-passes the pulmonary route of administration and allows for a high bolus dose of MWCNTs directly to the pleural cavity, whereas pulmonary exposure by inhalation or OPA likely result in a very low exposure of MWCNT in the pleural cavity via translocation through the pleural lymphatic drainage (Ryman-Rasmussen et al. 2009a). Rats appear to be more susceptible than mice as intratracheal instillation of rod-like MWCNTs into the lungs of F344 rats has been shown to cause mesothelioma (Suzui et al. 2016), a finding not yet seen in any strain of mouse exposed by direct pulmonary exposure to MWCNTs. Lung cancer but not mesothelioma was induced by the inhalation exposure of MWCNTs in rats (Kasai et al. 2016). Therefore, the method of pulmonary exposure (inhalation versus instillation) may be an important determinant of mesothelioma. Another caveat of our study is that

the sample size of approximately ten mice per group may be insufficient statistical power to determine a negative carcinogenic effect as recommended by IARC (IARC 2017). Despite the lack of lung or pleural tumors in the present study, we observed epithelial hyperplasia resulting from pulmonary exposure to rMWCNTs which agrees in part with previous studies that showed epithelial hyperplasia and adenocarcinoma in the lungs of MWCNT-exposed rodents (Sargent et al. 2014; Kasai et al. 2016).

The fibrogenic and carcinogenic potential of MWCNTs has been compared to asbestos, a class of naturally occurring mineral fibers represented by different types; some more rigid than others. For example, rMWCNTs or crocidolite, a rigid type of asbestos, both resulted in mesothelioma when injected intraperitoneally in C57BL/6 mice or Wistar rats and progression of mesothelioma in these animals was coupled with an accumulation of monocytic cells that suppressed polyclonal activation of lymphocytes 12 months following exposure (Huaux et al. 2016). The rMWCNTs used in that study were the same used in our current study. Therefore, rMWCNTs appear to behave similarly to rod-like crocidolite asbestos fibers. The rodent model is limited by a short life span (~2 years), and a latency period of over 15 years is common for asbestos-induced mesothelioma or fibrosis in humans (Frost 2013; Prazakova et al. 2014). Since our chronic study did not reveal mesothelioma, it may be possible that a longer time period might be required (between 12 and 24 months) for tumorigenesis after direct pulmonary exposure.

A variety of physicochemical characteristics likely play an important role in the inflammatory, fibrotic, and genotoxic responses to MWCNTs. Our study emphasized differences in nanotube geometry (i.e. tangled versus rod-like shape) although the two MWCNTs that we compared also had differences in other physicochemical characteristics such as length, surface area, surface charge, and residual metal catalyst content (Fe versus Ni). Other work has addressed physicochemical characteristics as predictors of disease outcome. For example, Poulsen et al. (2017) investigated the pulmonary exposure of 10 commercial MWCNTs in female C57BL/6J mice by intratracheal instillation and identified specific surface area (BET), length and surface

oxidation as predictors of pulmonary inflammation, whereas larger MWCNT diameter predicted genotoxicity in lung cells. Therefore, it is likely that multiple physicochemical features play a role in the pathologic responses to MWCNTs. In addition, it is also possible that physicochemical characteristics such as shape, length, and charge may influence agglomeration status and the number of nanotubes per unit mass. We dosed mice on a mass basis, but it is possible that this approach results in differences in the number of MWCNTs delivered to the lungs of mice.

Conclusions

Our findings show that genetic susceptibility (loss of one allele encoding the p53 tumor suppressor) plays a role in the immune response to MWCNT exposure in mice. A constitutively larger area of $CD45R^+/CD3^+$ lymphoid tissue was observed in the lungs of $p53^{+/-}$ mice compared to $p53^{+/+}$ mice and these mice had larger granulomas induced by either tMWCNTs or rMWCNTs as compared to $p53^{+/+}$ mice, with rMWCNTs causing the most prominent granuloma formation. While no lung or pleural tumors were observed in $p53^{+/-}$ mice after chronic MWCNT exposure, rMWCNTs caused greater epithelial cell hyperplasia in terminal bronchioles in both $p53^{+/-}$ and $p53^{+/-}$ mice. These findings indicate that both p53 deficiency and physicochemical features including nanotube geometry are factors in susceptibility to MWCNT-induced lymphoid infiltration and granuloma formation.

Acknowledgments

We are grateful for the help of Dr. Erinn Needham-Dandley for her expertise in TEM imaging of the as purchased MWCNTs.

Disclosure statement

No potential conflict of interest was reported by the authors.

Funding

References

Abdalla, S., F. Al-Marzouki, A. A. Al-Ghamdi, and A. Abdel-Daiem. 2.

Agarwal, M., A. Agarwal, W. Taylor, and G. Stark. 1995. "p53 Controls Both the G2/M and the G1 Cell Cycle Checkpoints and Mediates Reversible Growth Arrest in Human Fibroblasts." *Proceedings of the National Academy of Sciences of the United States of America* 92 (18): 8493–8497.

Aiso, S., K. Yamazaki, Y. Umeda, M. Asakura, T. Kasai, M. Takaya, T. Toya, S. Koda, K. Nagano, H. Arito, and S. Fukushima. 2010. "Pulmonary Toxicity of Intratracheally Instilled Multiwall Carbon Nanotubes in Male Fischer 344 Rats." *Industrial Health* 48 (6): 783–795.

Aloisi, F., and R. Pujol-Borrell. 2006. "Lymphoid Neogenesis in Chronic Inflammatory Diseases." *Nature Reviews Immunology* 6 (3): 205–217.

Barrett, J. C., P. W. Lamb, and R. W. Wiseman. 1989. "Multiple Mechanisms for the Carcinogenic Effects of Asbestos and Other Mineral Fibers." *Environmental Health Perspectives* 81: 81–89.

Bates, M. A., C. Brandenberger, I. Langohr, K. Kumagai, J. R. Harkema, A. Holian, and J. J. Pestka. 2015. "Silica Triggers Inflammation and Ectopic Lymphoid Neogenesis in the Lungs in Parallel with Accelerated Onset of Systemic Autoimmunity and Glomerulonephritis in the Lupus-Prone NZBWF1 Mouse." *PLoS One* 10 (5): e0125481. doi:10.1371/journal.pone.0125481.

Bozelka, B. E., P. Sestini, H. R. Gaumer, Y. Hammad, C. J. Heather, and J. E. Salvaggio. 1983. "A Murine Model of Asbestosis." *The American Journal of Pathology* 112 (3): 326–337.

Chernova, T., F. A. Murphy, S. Galavotti, X. M. Sun, I. R. Powley, S. Grosso, A. Schinwald, et al. 2017. "Long-Fiber Carbon Nanotubes Replicate Asbestos-Induced Mesothelioma with Disruption of the Tumor Suppressor Gene Cdkn2a (Ink4a/Arf)." *Current Biology* 27 (21): 3302–14.e6. doi:10.1016/j.cub.2017.09.007.

Dai, C., and W. Gu. 2010. "P53 Post-Translational Modification: Deregulated in *Tumorigenesis.*" *Trends in Molecular Medicine* 16 (11): 528–536. doi:10.1016/j.molmed.2010.09.002.

Dandley, E. C., A. J. Taylor, K. S. Duke, M. D. Ihrie, K. A. Shipkowski, G. N. Parsons, and J. C. Bonner. 2015. "Atomic Layer Deposition Coating of Carbon Nanotubes with Zinc Oxide Causes Acute Phase Immune Responses in Human Monocytes In Vitro and in Mice after Pulmonary Exposure." *Particle and Fibre Toxicology* 13 (1): 29. doi:10.1186/s12989-016-0141-9.

Donaldson, K., R. Aitken, L. Tran, V. Stone, R. Duffin, G. Forrest, and A. Alexander. 2006. "Carbon Nanotubes: A Review of Their Properties in Relation to Pulmonary Toxicology and Workplace Safety." *Toxicological Sciences* 92 (1): 5–22.

Dong, J., D. W. Porter, L. A. Batteli, M. G. Wolfarth, D. L. Richardson, and Q. Ma. 2015. "Pathologic and Molecular Profiling of Rapid - Onset Fibrosis and Inflammation Induced by Multi-Walled Carbon Nanotubes." *Archives of Toxicology* 89 (4): 621–633. doi:10.1007/s00204-014-1428-y.

Duke, K. S., and J. C. Bonner. 2018. "Mechanisms of Carbon Nanotube-Induced Pulmonary Fibrosis: A Physicochemical Characteristic Perspective." *Wiley Interdisciplinary Reviews: Nanomedicine and Nanobiotechnology* 10 (3): e1498. doi:10.1002/wnan.1498.

Duke, K. S., A. J. Taylor-Just, M. D. Ihrie, K. A. Shipkowski, E. A. Thompson, E. C. Dandley, G. N. Parsons, and J. C. Bonner. 2017. "STAT1-Dependent and -Independent Pulmonary Allergic and Fibrogenic Responses in Mice after Exposure to Tangled versus Rod-like Multi-Walled Carbon Nanotubes." *Particle and Fibre Toxicology* 14 (1): 26. doi:10.1186/s12989-017-0207-3.

Foo, S. Y., and S. Phipps. 2010. "Regulation of Inducible BALT Formation and Contribution to Immunity and Pathology." *Mucosal Immunology* 3 (6): 537–544. doi:10.1038/mi.2010.52.

Frost, G. 2013. "The Latency Period of Mesothelioma among a Cohort of British Asbestos Workers (1978-2005)." *British Journal of Cancer* 109 (7): 1965–1973. doi:10.1038/bjc.2013.514.

Goya, S., H. Matsuoka, M. Mori, H. Morishita, H. Kida, Y. Kobashi, T. Kato, et al. 2003. "Sustained Interleukin-6 Signalling Leads to the Development of Lymphoid Organ-like Structures in the Lung." *The Journal of Pathology* 200 (1): 82–87.

Hashimoto, D., A. Chow, C. Noizat, P. Teo, M. B. Beasley, M. Leboeuf, C. D. Becker, P. See, et al. 2013. "Tissue-Resident Macrophages Self-Maintain Locally throughout Adult Life with Minimal Contribution from Circulating Monocytes." *Immunity* 38 (4): 792–804. doi:10.1016/j.immuni.2013.04.004.

Hilton, G. M., A. J. Taylor, S. Hussain, E. C. Dandley, E. H. Griffith, S. Garantziotis, G. N. Parsons, J. C. Bonner, and M. S. Bereman. 2017. "Mapping Differential Cellular Protein Response of Mouse Alveolar Epithelial Cells to Multi-Walled Carbon Nanotubes as a Function of Atomic Layer Deposition Coating." *Nanotoxicology* 11 (3): 313–326. doi:10.1080/17435390.2017.1299888.

Hojo, S., J. Fujita, I. Yamadori, T. Kamei, T. Yoshinouchi, Y. Ohtsuki, H. Okada, et al. 1998. "Heterogeneous Point Mutations of the p53 Gene in Pulmonary Fibrosis." *The European Respiratory Journal* 12 (6): 1404–1408.

Hubbs, A. F., R. R. Mercer, S. A. Benkovic, J. Harkema, K. Sriram, D. Schwegler-Berry, M. P. Goravanahally, et al. 2011. "Nanotoxicology-A Pathologist's Perspective." *Toxicologic Pathology* 39 (2): 301–324. doi:10.1177/0192623310390705.

Huaux, F., V. d'Ursel de Bousies, M.-A. Parent, M. Orsi, F. Uwambayinema, R. Devosse, S. Ibouraadaten, et al. 2016. "Mesothelioma Response to Carbon Nanotubes Is Associated with an Early and Selective Accumulation of Immunosuppressive Monocytic Cells." *Particle and Fibre Toxicology* 13 (1): 46. doi:10.1186/s12989-016-0158-0.

Huizar, I., A. Malur, J. Patel, M. McPeek, L. Dobbs, C. Wingard, B. P. Barna, and M. J. Thomassen. 2013. "The Role of PPAR γ in Carbon Nanotube-Elicited Granulomatous Lung Inflammation." *Respiratory Research* 14 (1): 7. doi:10.1186/1465-9921-14-7.

Huizar, I., A. Malur, Y. A. Midgette, C. Kukoly, P. Chen, P. C. Ke, R. Podila, et al. 2011. "Novel Murine Model of Chronic Granulomatous Lung Inflammation Elicited by Carbon Nanotubes." *American Journal of Respiratory Cell and Molecular Biology* 45 (4): 858–866. doi:10.1165/rcmb.2010-0401OC.

Hunter, K. W. 2012. "Mouse Models of Cancer: Does the Strain Matter?" *Nature Reviews. Cancer* 12 (2): 144–149. doi:10.1038/nrc3206.

International Agency for Research on Cancer (IARC). 2017. "IARC Working Group on the Evaluation of Carcinogenic Risks to Humans." *Some Nanomaterials and Some Fibres*. Lyon, France: IARC.

John-Schuster, G., S. Günter, K. Hager, T. M. Conlon, O. Eickelberg, and A. Ö. Yildirim. 2015. "Inflammaging Increases Susceptibility to Cigarette Smoke-Induced COPD." *Oncotarget* 7: 30068–30083. doi:10.18632/oncotarget.4027.

Kasai, T., Y. Umeda, M. Ohnishi, T. Mine, H. Kondo, and T. Takeuchi. 2016. "Lung Carcinogenicity of Inhaled Multi-Walled Carbon Nanotube in Rats." *Part and Fibre Toxicology* 13: 1–19.

Købler, C., S. S. Poulsen, A. T. Saber, N. R. Jacobsen, H. Wallin, C. L. Yauk, S. Halappanavar, U. Vogel, K. Qvortrup, and K. Mølhave. 2015. "Time-Dependent Subcellular Distribution and Effects of Carbon Nanotubes in Lungs of Mice." *PLoS One* 10 (1): e0116481. doi:10.1371/journal.pone.0116481.

Kuroda, E., K. Ozasa, B. Temizoz, K. Ohata, C. X. Koo, T. Kanuma, T. Kusakabe, et al. 2016. "Inhaled Fine Particles Induce Alveolar Macrophage Death and Interleukin-1α Release to Promote Inducible Bronchus-Associated Lymphoid Tissue Formation." *Immunity* 45 (6): 1299–1310. doi:10.1016/j.immuni.2016.11.010.

Lowe, J. M., D. Menendez, P. R. Bushel, M. Shatz, E. L. Kirk, and M. A. Troester. 2014. "p53 and NF-κB Coregulate Proinflammatory Gene Responses in Human Macrophages." *Cancer Research* 74: 2182–2192. doi:10.1158/0008-5472.CAN-13-1070.

Madenspacher, J. H., K. M. Azzam, K. M. Gowdy, K. C. Malcolm, J. A. Nick, D. Dixon, J. J. Aloor, et al. 2013. "P53 Integrates Host Defense and Cell Fate during Bacterial Pneumonia." *The Journal of Experimental Medicine* 210 (5): 891–904. doi:10.1084/jem.20121674.

Mercer, R. R., J. F. Scabilloni, A. F. Hubbs, L. Wang, L. A. Battelli, W. McKinney, V. Castranova, and D. W. Porter.

2013. "Extrapulmonary Transport of MWCNT following Inhalation Exposure." *Particle and Fibre Toxicology* 10 (1): 38. doi:10.1186/1743-8977-10-38.

Mercer, R. R., A. F. Hubbs, J. F. Scabilloni, L. Wang, L. A. Batteli, S. Friend, V. Castranova, and D. W. Porter. 2011. "Pulmonary Fibrotic Response to Aspiration of Multi-Walled Carbon Nanotubes." *Particle and Fibre Toxicology* 8 (1): 21. doi:10.1186/1743-8977-10-38.

Muller, J., F. Huaux, N. Moreau, P. Misson, J.-F. Heilier, M. Delos, M. Arras, A. Fonseca, J. B. Nagy, and D. Lison. 2005. "Respiratory Toxicity of Multi-Wall Carbon Nanotubes." *Toxicology and Applied Pharmacology* 207 (3): 221–231.

Murphy, F., A. Schinwald, C. Poland, and K. Donaldson. 2012. "The Mechanism of Pleural Inflammation by Long Carbon Nanotubes: interaction of Long Fibres with Macrophages Stimulates Them to Amplify Pro-Inflammatory Responses in Mesothelial Cells." *Particle and Fibre Toxicology* 9 (1): 8. doi:10.1186/1743-8977-9-8.

Murphy, J., R. Summer, A. A. Wilson, D. N. Kotton, and A. Fine. 2008. "The Prolonged Life-Span of Alveolar Macrophages." *American Journal of Respiratory Cell and Molecular Biology* 38 (4): 380–385. doi:10.1165/rcmb.2007-0224RC.

Nagai, H., Y. Okazaki, S. H. Chew, N. Misawa, Y. Yamashita, S. Akatsuka, T. Ishihara, et al. 2011. "Diameter and Rigidity of Multiwalled Carbon Nanotubes Are Critical Factors in Mesothelial Injury and Carcinogenesis." *Proceedings of the National Academy of Sciences of the United States of America* 108 (49): E1330–E1338. doi:10.1073/pnas.1110013108.

Neyt, K., C. H. GeurtsvanKessel, K. Deswarte, H. Hammad, and B. N. Lambrecht. 2016. "Early IL-1 Signaling Promotes iBALT Induction after Influenza Virus Infection." *Frontiers in Immunology* 7: 312. doi:10.3389/fimmu.2016.00312.

Ohtani, H. 2013. "Granuloma Cells in Chronic Inflammation Express CD205 (DEC205) Antigen and Harbor Proliferating T Lymphocytes: Similarity to Antigen-Presenting Cells." *Pathology International* 63 (2): 85–93. doi:10.1111/pin.12036.

Poland, C. A., R. Duffin, I. Kinloch, A. Maynard, W. A. H. Wallace, A. Seaton, V. Stone, S. Brown, W. MacNee, and K. Donaldson. 2008. "Carbon Nanotubes Introduced into the Abdominal Cavity of Mice Show Asbestos-like Pathogenicity in a Pilot Study." *Nature Nanotechnology* 3 (7): 423–428. doi:10.1038/nnano.2008.111.

Porter, D. W., A. F. Hubbs, R. R. Mercer, N. Wu, M. G. Wolfarth, K. Sriram, S. Leonard, et al. 2010. "Mouse Pulmonary Dose- and Time Course-Responses Induced by Exposure to Multi-Walled Carbon Nanotubes." *Toxicology* 269 (2–3): 136–147.

Poulsen, S. S., P. Jackson, K. Kling, K. B. Knudsen, V. Skaug, Z. O. Kyjovska, B. L. Thomsen, et al. 2017. "Multi-Walled Carbon Physicochemical Properties Predict Pulmonary Inflammation and Genotoxicity." *Nanotoxicology* 10 (10): 1263–1275. doi:10.1371/journal.pone.0174167.

Prazakova, S., P. S. Thomas, A. Sandrini, and D. H. Yates. 2014. "Asbestos and the Lung in the 21st Century: An

Update." *The Clinical Respiratory Journal* 8 (1): 1–10. doi:10.1111/crj.12028.

Preibisch, S., S. Saalfeld, and P. Tomancak. 2009. "Globally Optimal Stitching of Tiled 3D Microscopic Image Acquisitions." *Bioinformatics* 25 (11): 1463–1465. doi:10.1093/bioinformatics/btp184.

Renne, R., A. Brix, J. Harkema, R. Herbert, B. Kittel, D. Lewis, T. March, et al. 2009. "Proliferative and Nonproliferative Lesions of the Rat and Mouse Respiratory Tract." *Toxicologic Pathology* 37 (Suppl. 7): 5S–73S. doi:10.1177/0192623309353423.

Rittinghausen, S., A. Hackbarth, O. Creutzenberg, H. Ernst, U. Heinrich, A. Leonhardt, and D. Schaudien. 2014. "The Carcinogenic Effect of Various Multi-Walled Carbon Nanotubes (MWCNTs) after Intraperitoneal Injection in Rats." *Particle and Fibre Toxicology* 11 (1): 59. doi:10.1186/s12989-014-0059-z.

Ryman-Rasmussen, J. P., M. F. Cesta, A. R. Brody, J. K. Shipley-Phillips, J. I. Everitt, E. W. Tewksbury, O. R. Moss, et al. 2009a. "Inhaled Carbon Nanotubes Reach the Subpleural Tissue in Mice ." *Nature Nanotechnology* 4 (11): 747–751. doi:10.1038/nnano.2009.305.

Ryman-Rasmussen, J. P., E. W. Tewksbury, O. R. Moss, M. F. Cesta, B. A. Wong, and J. C. Bonner. 2009b. "Inhaled Multiwalled Carbon Nanotubes Potentiate Airway Fibrosis in Murine Allergic Asthma." *American Journal of Respiratory Cell and Molecular Biology* 40 (3): 349–358. doi:10.1165/rcmb.2008-0276OC.

Sakamoto, Y., D. Nakae, N. Fukumori, K. Tayama, A. Maekawa, K. Imai, A. Hirose, T. Nishimura, N. Ohashi, and A. Ogata. 2009. "Induction of Mesothelioma by a Single Intrascrotal Administration of Multi-Wall Carbon Nanotube in Intact Male Fischer 344 Rats." *The Journal of Toxicological Sciences* 34 (1): 65–76.

Sargent, L. M, D. W. Porter, L. M. Staska, A. F. Hubbs, D. T. Lowry, L. Battelli, K. J. Siegrist, et al. 2014. "Promotion of Lung Adenocarcinoma following Inhalation Exposure to Multi-Walled Carbon Nanotubes." *Particle and Fibre Toxicology* 11 (1): 3. doi:10.1186/1743-8977-11-3.

Schneider, C. A., W. S. Rasband, and K. W. Eliceiri. 2012. "NIH Image to ImageJ: 25 Years of Image Analysis." *Nature Methods* 9 (7): 671–675.

Siegrist, K. J., S. H. Reynolds, M. L. Kashon, D. T. Lowry, C. Dong, A. F. Hubbs, S.-H. Young, et al. 2014. "Genotoxicity of Multi-Walled Carbon Nanotubes at Occupationally Relevant Doses." *Particle and Fibre Toxicology* 11 (1): 6. doi:10.1186/1743-8977-11-6.

Sminia, T., G. J. van der Brugge-Gamelkoorn, and S. H. Jeurissen. 1989. "Structure and Function of Bronchus-Associated Lymphoid Tissue (BALT)." *Critical Reviews in Immunology* 9 (2): 119–150.

Suzui, M., M. Futakuchi, K. Fukamachi, T. Numano, M. Abdelgied, S. Takahashi, M. Ohnishi, et al. 2016. "Multiwalled Carbon Nanotubes Intratracheally Instilled into the Rat Lung Induce Development of Pleural Malignant Mesothelioma and Lung Tumors." *Cancer Science* 107 (7): 924–935. doi:10.1111/cas.12954.

Takagi, A., A. Hirose, T. Nishimura, N. Fukumori, A. Ogata, N. Ohashi, S. Kitajima, and J. Kanno. 2008. "Induction of Mesothelioma in p53+/- Mouse by Intraperitoneal Application of Multi-Wall Carbon Nanotube." *The Journal of Toxicological Sciences* 33 (1): 105–116.

Takagi, A., A. Hirose, M. Futakuchi, H. Tsuda, and J. Kanno. 2012. "Dose-Dependent Mesothelioma Induction by Intraperitoneal Administration of Multi-Wall Carbon Nanotubes in p53 Heterozygous Mice." *Cancer Science* 103 (8): 1440–1444. doi:10.1111/j.1349-7006.2012.02318.x.

Takahashi, T., M. Munakata, Y. Ohtsuka, H. Nisihara, Y. Nasuhara, A. Kamachi-Satoh, H. Dosaka-Akita, Y. Homma, and Y. Kawakami. 2002. "Expression and Alteration of Ras and p53 Proteins in Patients with Lung Carcinoma Accompanied by Idiopathic Pulmonary Fibrosis." *Cancer* 95 (3): 624–633.

Vancheri, C., M. Failla, N. Crimi, and G. Raghu. 2010. "Idiopathic Pulmonary Fibrosis: A Disease with Similarities and Links to Cancer Biology." *The European Respiratory Journal* 35 (3): 496–504. doi:10.1183/09031936.00077309.

Wang, Y., Z. Zhang, R. A Lubet, and M. You. 2006. "A Mouse Model for Tumor Progression of Lung Cancer in Ras and p53 Transgenic Mice." *Oncogene* 25 (8): 1277–1280.

Wang, Y., Y.-A. H. Suh, M. Y. Fuller, J. G. Jackson, S. Xiong, T. Terzian, A. Quintás-Cardama, J. A. Bankson, A. K. El-Naggar, and G. Lozano. 2011. "Restoring Expression of Wild-Type p53 Suppresses Tumor Growth but Does Not Cause Tumor Regression in Mice with a p53 Missense Mutation." *Journal of Clinical Investigation* 121 (3): 893–904. doi:10.1172/JCI44504.

Xu, B., J. F. Guenther, D. A. Pociask, Y. Wang, J. K. Kolls, Z. You, B. Chandrasekar, B. Shan, D. E. Sullivan, and G. F. Morris. 2014. "Promotion of Lung Tumor Growth by Interleukin-17." *American Journal of Physiology. Lung Cellular and Molecular Physiology* 307 (6): L497–L508. doi:10.1152/ajplung.00125.2014.

Xu, J., M. Futakuchi, H. Shimizu, D. B. Alexander, K. Yanagihara, K. Fukamachi, M. Suzui, et al. 2012. "Multi-Walled Carbon Nanotubes Translocate into the Pleural Cavity and Induce Visceral Mesothelial Proliferation in Rats." *Cancer Science* 103 (12): 2045–2050. doi:10.1111/cas.12005.

Xu, J., D. B. Alexander, M. Futakuchi, T. Numano, K. Fukamachi, M. Suzui, T. Omori, J. Kanno, A. Hirose, and H. Tsuda. 2014b. "Size- and Shape-Dependent Pleural Translocation, Deposition, Fibrogenesis, and Mesothelial Proliferation by Multiwalled Carbon Nanotubes." *Cancer Science* 105 (7): 763–769. doi:10.1111/cas.12437.

Zilfou, J. T., and S. W. Lowe. 2009. "Tumor Suppressive Functions of p53." *Cold Spring Harbor Perspectives in Biology* 1 (5): a001883. doi:10.1101/cshperspect.a001883.